

Rural Optical-Propagation Measurements

Bernhard EPPLE¹, Hennes HENNIGER², Stefan KURZ³, Hubertus HAAN³

¹Institute of Communications and Navigation, German Aerospace Center (DLR), 82234 Wessling, Germany

²Codex GmbH & Co. KG, 82211 Herrsching, Germany

³Carl Zeiss Optronics GmbH, 73447 Oberkochen, Germany

bernhard.epple@dlr.de

Abstract. *Compared with traditional communication technologies like wired or radio frequency communications, optical wireless communication has a unique fading behavior of the received signal, that does not allow to use existing channel models without modification. In this paper the statistics of received optical power obtained from experimental data are compared to often used statistical mathematical models. These models are the log-normal and the gamma-gamma distribution. It was found that the gamma-gamma gives better fits to the measured data, but the quality of the log-normal fits is sufficient for most needs. This means that the log-normal distribution can be used for the development of simplified channel models which have a better mathematical tractability than the models based on the gamma-gamma distribution.*

Keywords

Optical wireless, communications, measurement, channel model, free-space, FSO, OWC.

1. Introduction

The most significant difference between optical wireless communications (OWC) and traditional communication technologies like wired or radio frequency communications is the unique fading behavior of the received signal. The experienced fades have typically durations up to 100 ms or longer and exceed easily the duration of several thousand bits. This special behavior requires modifications of existing channel models if they should be applied to OWC. The two most often used distributions for modeling the received optical power are the log-normal (LN) and gamma-gamma (GG) distribution [1], [2], [3], where scientists in general prefer the LN distribution because of its better mathematical tractability, but the GG distribution should lead to more accurate results. In real world communications systems there are also additional components that influence the distribution of the received power, e.g. the accuracy of the used tracking system in mobile scenarios. Therefore even if one of the proposed distributions would result in a perfect fit for the distribution of the received power, a deviation from this dis-

tribution would be visible in a real world scenario. In order to model the optical channel it is nearly impossible to give a distribution of the received power for all situations and channel conditions but it is important to identify power distributions that result in a fit with real world data with a sufficient accuracy.

This paper is organized as follows. In Section 2 the measurement scenario is described in detail. In Section 3.1 the methodology of fitting the two distributions is described and in Section 3.2 the results of the fitting are presented. In addition to the results from the curve fitting analysis additional measured parameters like power scintillation index and channel correlation time are given in 3.3. In 4 the turbulence regime during the measurements and the effect of aperture averaging are investigated. In Section 5 parameters for reproducing the measurements using a simplified channel model are given before the paper is concluded in Section 6.

2. The Measurement Scenario

The presented measurements were taken in the vicinity of Ellwangen, Germany, in June 2010. A diverged Gaussian beam (full width half maximum divergence 1.1 mrad) at 1550 nm wavelength was propagated nearly horizontally, near ground, through different regimes of index-of-refraction turbulence. The transmitter was located about 0.5 m above the ground, whereas the receiver was located at four different locations around Ellwangen (see. Fig. 1), about 1 m above the ground.

Over most of the path the link was passing over grassland. The path length between the transmitter and the four measurement locations was between 3.8 km and 16.6 km. As transmitter the Laser Communication Terminal for Marine Environment (LCT-Marine) provided by Carl Zeiss Optronics was used. The stabilized LCT-Marine tracking platform kept the pointing error below 100 μ rad. A 300 mm focal length refractive receiving telescope with an aperture of 9 cm was mounted on an azimuth-elevation pointing head on top of a tripod. For measurements a set of circular stops were used to vary the working aperture between 2.5 cm, 5 cm, 7.5 cm and 9 cm. These aperture sizes were chosen in a way to ensure a good signal-to-noise ratio of the received power at all link distances and aperture sizes. The receiver system

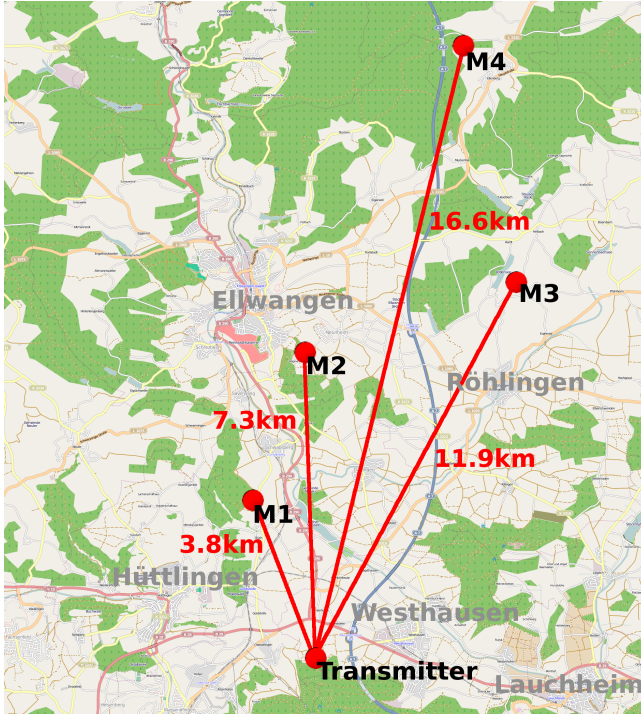


Fig. 1. Map of the transmitter and receiver positions (M1-M4) for the experiment. The numbers beside the lines give the link distance in kilometers. (source: OpenStreetMap).

full angle field of view was limited to approximately 3 mrad. A Thorlabs PDA10CS detector module was used to convert the optical received power into an electrical signal which was sampled with a 16 bit analog digital converter. From previous scintillation measurements performed with similar setups [3], [4] and from literature [5], [2] it is known that the received power does not have any spectral components above approximately 2000 Hz. So data collection at 6100 Hz was used, as this rate would be sufficient to capture any small scale fluctuation in the signal.

Before and after each measurement run a measurement of the background light was performed in order to subtract the average background light plus any electronic bias in post processing. For each aperture size, three power measurements with a duration of one second were done immediately after each other.

Weather conditions during measurements at transmitter and the four receiver locations: about 20 °C with overcast sky. The orthogonal wind speed was about the same at all locations with variation between 1 m/s and 5 m/s. The visibility was estimated to be about 10 km.

3. Received Power Statistics

In this section the suitability of LN and GG to describe the amplitude variation of the received power is investigated. Further, some tables and figures are presented to illustrate the measured parameters as well as fit-results for all taken measurements.

3.1 Fitting Technique and Estimation of Fitting Error

For fitting the two distributions against the measured data, the same methodology as in [3] has been applied. For fitting the LN distribution to the measurement data the parameters of the LN distribution can be directly calculated from the measured data but the parameters of the GG distribution have to be determined by a search as it is described in [3]. After the parameters for the distributions have been determined from the measurements, following error measures are used to evaluate the quality of the fit.

$$\mathbf{e} = F_M(P_{Rx}) - F(P_{Rx}), \quad (1)$$

$$e_{abs} = \max(|\mathbf{e}|), \quad (2)$$

$$e_{rms} = \sqrt{\langle \mathbf{e}^2 \rangle}, \quad (3)$$

$$e_{rel} = \left\langle \frac{\mathbf{e}}{F(P_{Rx})} \right\rangle \quad (4)$$

where $F(P_{Rx})$ is the cumulative distribution function (CDF) of either LN or GG distribution and $F_M(P_{Rx})$ is the empirical CDF derived from the measured data. \mathbf{e} is the error vector between measurement and fit, e_{abs} is the maximum absolute error, e_{rms} is the root mean squared error and e_{rel} is the mean relative error between the two curves.

The CDF is used for the evaluation of the fit because its empirical form can be derived from the measured data easily by sorting the measured values, calculating the cumulative sum of the measured values and normalizing it by the maximum value. To derive the probability distribution function (PDF) the histogram of the measured data has to be generated, which involves sorting the measured values into a given number of bins. Then the histogram has to be normalized by an estimate of its area, to form the empirical PDF. Both steps, the binning as well as the estimation of the area of the histogram, will add inaccuracies to the evaluation results.

The three introduced error values are used in the following way: e_{abs} is used to visualize the maximum distance between the distributions and the measurements. e_{rms} is used to evaluate how well the distribution agrees over the whole range of the measured values. e_{abs} and e_{rms} are linear error measures that will produce larger error values in regions where the distributions have larger values. Therefore, fitting errors at the lower values of the CDF are more or less ignored. To visualize errors for lower values, e_{rel} is used which relates the fitting error to the value of the distribution. This error measure is also used to determine the best fitting distribution.

3.2 LN and GG Fit

Tab. 3 shows fit-errors for the GG and LN distribution which were fit against the measurements. The distribution which fits the measurement data better is given in the second last column of the table. The decision about the best fit is based on e_{rel} , because only this error measure takes

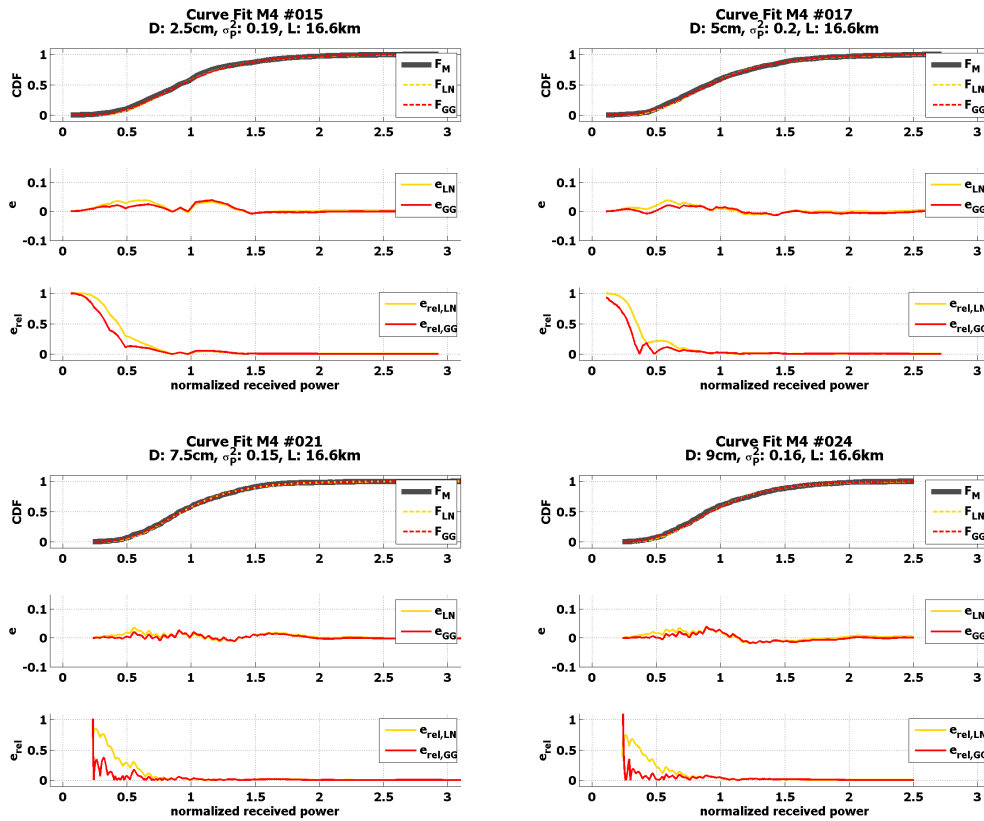


Fig. 2. Exemplary curve fit results for measurements at location M4. Each subfigure shows a plot of F_M and F in the upper part and below plots of e and e_{rel} for the measurements taken with different aperture sizes (D). For e_{rel} only the fraction from (4) is shown. The title of each plot gives the measurement location (M4) and a running number for that particular measurement. L is the link distance.

the fitting errors also for lower values into account. It can be clearly seen that GG is most often the best fit (90 % of all measurements). Nevertheless for LN the fit-errors are within an acceptable range for all aperture sizes and link distances; e_{rms} is always less than 0.035. A comparison between the fits of LN and GG is shown in Fig. 2.

For all plots it can be seen that e_{rel} emphasizes the fitting errors in the lower region. This fitting error is supposed to be produced by a lower signal-to-noise ratio for lower signal levels. For the two smaller apertures the absolute received power was lower and therefore, the signal-to-noise ratio was worse than for the two larger aperture sizes. This error is driven by the detector noise and therefore its behavior is similar for LN and GG.

The measurements confirm that theory provided by [1], [2] which suggest GG for modeling the dynamics of the received power for long-range optical wireless links is valid. Nevertheless, it shows that also LN, which is in general only applied for short-range links and weak turbulence regime, can be used. This observation has also been recently made based on measurements from different environments [3], [4]. The importance of the LN distribution for the optical wireless engineering society is based on its simple mathematical tractability. This feature is important for engineers which need to model such process in order to set up system test channel simulators. A concept for such a simulator is pre-

sented in [3] and shall not be repeated here. Further with the LN model the fading loss can easily be calculated which is important for link-budget calculations [6].

3.3 Discussion on Measured Parameters

Tab. 3 at the end of this publication gives the power scintillation index σ_p^2 for the different path lengths L and for different receiver aperture sizes D . If all measurements are compared by σ_p^2 in general a reduction of σ_p^2 for larger D can be observed. This effect is well known as aperture averaging which will be discussed in more detail in the next section. The last column shows the channel correlation time τ which is defined as the time after which the autocorrelation function has dropped by 50 %. The channel correlation time indicates that for optical links in a rural environment fade durations of up to over 30 ms can be expected.

4. Aperture Averaging

For an interpretation of the measurement results it is important to know the scintillation index σ_I^2 that was present during the measurements. For estimation of σ_I^2 the well known aperture averaging factor A_{AF} can be used. A_{AF} is generally defined as:

$$A_{AF} = \frac{\sigma_P^2}{\sigma_I^2}. \quad (5)$$

For the measurements it is expected that the transmitted beam can be approximated by a plane wave, because of the relatively long propagation distances. For a plane wave under weak turbulence conditions A_{AF} can be calculated by [7]:

$$A_{AF}(D) = \left(1 + 1.062 \frac{kD^2}{4L}\right)^{-7/8}; 0 < A_{AF}(D) < 1 \quad (6)$$

where $k = 2\pi/\lambda$ is the wave number, λ is the wavelength, D is the diameter of the receiving aperture and L is the link distance. Eq. (5) and (6) can be used to estimate σ_I^2 from the measured σ_P^2 values. Doing so, four different values for σ_I^2 were derived for the four different aperture sizes at each measurement location. The mean value of these four estimates is given in the first column of Tab. 2 for all measurement locations (M1-M4). The other columns in Tab. 2 give the derived estimates for the four different aperture sizes at the four measurement locations. A generally used definition for weak turbulence is $\sigma_I^2 < 0.3$ and for moderate-to-strong scintillation $\sigma_I^2 > 0.3$. From this it can be concluded that the measurements were taken under moderate-to-strong turbulence conditions, except M4, where weak turbulence was present. The reduction of σ_I^2 for M4 is most likely caused by a drop of C_n^2 as this measurement was taken during sunset where atmospheric effects are known to calm down. The estimated σ_I^2 has been used to calculate the apparent A_{AF} for each aperture size using Eq. (5). The result of this is shown in Fig. 3. Because of the way these values were generated, they can only be used as a rough estimation to illustrate the development of A_{AF} over the link distance, but they can not be used as exact measurement results. From these plots it can be seen that the measured A_{AF} follows the theoretical curve very well although a formula only valid under weak turbulence has been used. This implies that (6) can not be used for calculating A_{AF} under all turbulence conditions, but to derive an estimate.

5. Channel Model Parameters

In [3] a simplified channel model has been presented for simulation of the optical channel. The basic concept of this channel model is that if the received power is LN distributed, it can be simulated by generating a set of normally distributed random numbers and filtering them with an appropriate low-pass filter. It has been shown in Section 3.2 that assumption of LN distributed received power should be accurate enough for the presented measurements and therefore this channel model can be applied. One parameter required as input to the model is σ_P^2 which has already been given in Tab. 3. Another input parameter is the filter that should be applied, which is given in Tab. 1. As it can be seen a first order Bessel filter with a cut-off frequency (f_C) between 59 and 199 Hz should be suitable to reproduce the measured channel. An interesting observation is that the best filter type and also f_C do not depend on the link distance. For

a more detailed description of the model and the selection of the filters refer to [3].

Location (#samples)	Filter	Order	f_C (Hz)	%
M1 (24)	Bessel	1	59-120	88
	Tatarskii	-	60-62	8
	Bessel	2	338	4
M2 (24)	Bessel	1	59-83	79
	Bessel	2	160-409	21
	Tatarskii	-	-	-
M3 (24)	Bessel	1	59-84	67
	Bessel	2	122-247	30
	Tatarskii	-	59	3
M4 (24)	Bessel	1	59-199	96
	Bessel	2	309	4
	Tatarskii	-	-	-

Tab. 1. Channel model parameters for the four measurement locations. The column % gives the percentage of how often this filter type produced the best fitting results in the evaluation.

6. Summary and Conclusion

In this paper results of channel measurements from four long-range horizontal optical links in rural area were presented. It could be shown that the gamma-gamma model known from scintillation theory is in good agreement with the measured data. Nevertheless, the log-normal distribution also shows a sufficient fitting quality with a root mean squared error of less than 0.035 in various scintillation regimes and for different aperture sizes. Therefore the log-normal distribution is a distribution with good mathematical tractability which can be used for modeling the optical wireless channel. Additionally the fade duration has been evaluated to be in the range of up to 30 ms. Further a quick look on the theory regarding the aperture averaging factor has been taken and it has been shown, that the measured values are in good agreement with this theory. Finally, parameters for a simplified channel model are given so the measured values can be reproduced for simulations.

References

- [1] ANDREWS, L. C., PHILLIPS, R. L. *Laser Beam Propagation through Random Media, Second Edition*. SPIE Press Monograph vol. PM152, 2005.
- [2] MAJUMDAR, A. K., RICKLIN, J. C. *Free-Space Laser Communications Principles and Advances*. Berlin: Springer, 2008.
- [3] EPPLE, B. A simplified channel model for simulation of free-space optical communications. *IEEE/OSA Journal of Optical Communications and Networking*, 2010, vol. 2, no. 5, p. 293 - 304.
- [4] HENNIGER, H., EPPLE, B., HAAN, H. Maritime mobile optical-propagation channel measurements. In *Proceedings of IEEE International Conference on Communications IEEE ICC 2010*. Cape Town (RSA), 2010.

[5] KARP, S., GAGLIARDI, R. M., MAORAN, E. S., STOTTS, L. B. *Optical Channels: Fibers, Clouds, Water, and the Atmosphere*. Plenum Press, 1988.

[6] HENNIGER, H., WILFERT, O. An introduction to free-space op-

tical communications. *Radioengineering*, 2010, vol. 19, no. 2, p. 203 - 212.

[7] ANDREWS, L. C. *Field Guide to Atmospheric Optics*. Bellingham (USA): SPIE Press, 2004.

	σ_I^2	$A_{AF}(0.025)$	$A_{AF}(0.05)$	$A_{AF}(0.075)$	$A_{AF}(0.09)$
M1	0.62	0.94	0.70	0.36	0.34
M2	0.84	1.00	0.73	0.56	0.51
M3	0.67	0.99	0.92	0.72	0.52
M4	0.21	0.86	0.93	0.74	0.74

Tab. 2. Estimated values for σ_I^2 and $A_{AF}(D)$.

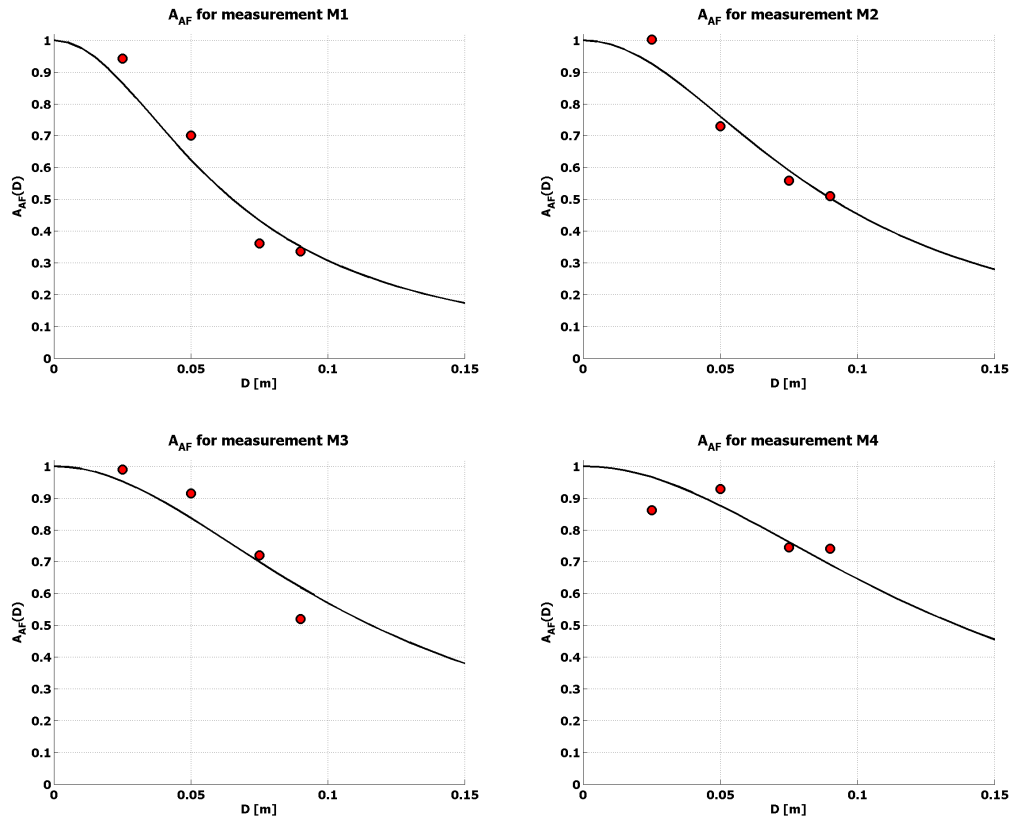


Fig. 3. Comparison between theoretical A_{AF} (black line) according to Eq. (6) and A_{AF} (red dots) calculated from the measurements.

ID	L (m)	D (m)	σ_p^2	$e_{rms,LN}$	$e_{abs,LN}$	$e_{rel,LN}$	$e_{rms,GG}$	$e_{abs,GG}$	$e_{rel,GG}$	Best Fit	τ (ms)
M1.013	3778	0.025	0.5	0.026	0.103	0.087	0.018	0.068	0.059	GG	6
M1.014	3778	0.025	0.6	0.035	0.116	0.089	0.023	0.087	0.064	GG	8
M1.015	3778	0.025	0.6	0.021	0.093	0.055	0.015	0.066	0.038	GG	7
M1.016	3778	0.05	0.6	0.021	0.072	0.052	0.012	0.055	0.021	GG	7
M1.017	3778	0.05	0.4	0.014	0.057	0.052	0.012	0.048	0.022	GG	7
M1.018	3778	0.05	0.3	0.013	0.064	0.046	0.010	0.038	0.034	GG	8
M1.019	3778	0.075	0.2	0.008	0.037	0.061	0.006	0.017	0.033	GG	7
M1.020	3778	0.075	0.2	0.013	0.040	0.053	0.010	0.033	0.089	LN	7
M1.021	3778	0.075	0.2	0.017	0.054	0.112	0.011	0.036	0.066	GG	9
M1.022	3778	0.09	0.2	0.009	0.031	0.051	0.010	0.034	0.030	GG	8
M1.023	3778	0.09	0.2	0.010	0.027	0.050	0.008	0.029	0.047	GG	9
M1.024	3778	0.09	0.2	0.022	0.069	0.080	0.016	0.049	0.044	GG	7
M2.013	7321	0.025	0.7	0.021	0.098	0.058	0.010	0.050	0.031	GG	7
M2.014	7321	0.025	1.0	0.022	0.125	0.037	0.010	0.067	0.018	GG	7
M2.015	7321	0.025	0.8	0.034	0.132	0.073	0.020	0.083	0.044	GG	7
M2.016	7321	0.05	0.5	0.021	0.102	0.072	0.014	0.067	0.049	GG	8
M2.017	7321	0.05	0.8	0.019	0.080	0.049	0.011	0.039	0.034	GG	9
M2.018	7321	0.05	0.5	0.022	0.072	0.083	0.012	0.037	0.044	GG	8
M2.019	7321	0.075	0.4	0.017	0.062	0.065	0.013	0.036	0.092	LN	10
M2.020	7321	0.075	0.5	0.020	0.077	0.077	0.012	0.044	0.051	GG	10
M2.021	7321	0.075	0.5	0.018	0.059	0.074	0.013	0.042	0.039	GG	10
M2.022	7321	0.09	0.4	0.015	0.064	0.084	0.008	0.036	0.049	GG	9
M2.023	7321	0.09	0.5	0.009	0.046	0.039	0.006	0.024	0.016	GG	11
M2.024	7321	0.09	0.4	0.016	0.067	0.086	0.009	0.039	0.057	GG	9
M3.013	11974	0.025	0.6	0.017	0.082	0.053	0.010	0.050	0.036	GG	21
M3.014	11974	0.025	0.7	0.017	0.067	0.047	0.016	0.065	0.026	GG	12
M3.015	11974	0.025	0.7	0.019	0.071	0.059	0.018	0.056	0.033	GG	20
M3.016	11974	0.05	1.0	0.013	0.044	0.025	0.022	0.089	0.051	LN	24
M3.017	11974	0.05	0.4	0.033	0.108	0.079	0.023	0.076	0.049	GG	14
M3.018	11974	0.05	0.4	0.009	0.033	0.060	0.012	0.040	0.038	GG	21
M3.019	11974	0.075	0.7	0.013	0.050	0.048	0.021	0.072	0.052	LN	28
M3.020	11974	0.075	0.4	0.028	0.074	0.127	0.019	0.046	0.096	GG	23
M3.021	11974	0.075	0.4	0.027	0.062	0.129	0.021	0.043	0.096	GG	21
M3.022	11974	0.09	0.4	0.028	0.072	0.137	0.021	0.045	0.107	GG	23
M3.023	11974	0.09	0.3	0.024	0.068	0.133	0.017	0.040	0.095	GG	23
M3.024	11974	0.09	0.3	0.024	0.073	0.099	0.017	0.050	0.044	GG	31
M4.013	16628	0.025	0.2	0.017	0.056	0.166	0.012	0.040	0.135	GG	10
M4.014	16628	0.025	0.2	0.013	0.037	0.104	0.011	0.028	0.067	GG	9
M4.015	16628	0.025	0.2	0.016	0.038	0.143	0.014	0.039	0.114	GG	9
M4.016	16628	0.05	0.2	0.008	0.020	0.092	0.008	0.023	0.056	GG	10
M4.017	16628	0.05	0.2	0.012	0.039	0.117	0.009	0.021	0.077	GG	11
M4.018	16628	0.05	0.2	0.027	0.060	0.202	0.023	0.051	0.167	GG	10
M4.019	16628	0.075	0.2	0.024	0.066	0.151	0.019	0.050	0.116	GG	10
M4.020	16628	0.075	0.2	0.015	0.044	0.082	0.013	0.041	0.049	GG	10
M4.021	16628	0.075	0.2	0.010	0.036	0.067	0.007	0.028	0.023	GG	10
M4.022	16628	0.09	0.2	0.010	0.034	0.035	0.011	0.039	0.044	LN	10
M4.023	16628	0.09	0.1	0.019	0.045	0.148	0.015	0.040	0.116	GG	9
M4.024	16628	0.09	0.2	0.014	0.040	0.085	0.011	0.039	0.031	GG	11

Tab. 3. Tabular listing of the curve fit results for the LN and GG distribution.